Progress In Electromagnetics Research, Vol. 143, 463–483, 2013

CHARACTERIZATION AND INVESTIGATION OF COMPOSITE RESISTIVE GRATING

Cheng Yuan Chin* **and Christina F. Jou**

Department of Electrical Engineering, National Chiao-Tung University, 1001 University Road, Hsinchu, Taiwan, R.O.C.

Abstract—A novel composite resistive grating is presented. It is formed by combining two complementary resistive patterns. The problem of plane wave scattering by a two-dimensional resistive grating is considered. The formulation involves the concept of Fourier series expansion, which is manipulated to deal with the resistive boundary condition. The advantage of the formulation comparing with method of moments is that it can solve grating having arbitrary admittance distribution without doing reformulation process. Both conventional and composite resistive gratings are numerically investigated and characterized. Additionally, the equivalent circuit models of one-dimensional resistive gratings are acquired for TE and TM polarizations. Finally, the design of multilayered Jaumann absorbers incorporating conventional or composite resistive gratings are taken as numerical examples, where the accuracy of equivalent circuit models are verified. The proposed composite grating can increase the originally unavoidable small gap width from 0.1 mm to 0.4 mm in the Jaumann absorber design, which is proved to possess more design flexibility and higher tolerance to fabrication error than conventional one.

1. INTRODUCTION

Electromagnetic wave scattering problem of periodic structures has been extensively studied from early on. Periodic arrays made of metal or dielectric have been widely used in a variety of applications including frequency selective filters, beam polarizers, or dichroic subreflectors.

Many studies have dealt with the analysis of metallic gratings [1, 2]. Except exclusive use of perfect electric conductor (PEC),

Received 25 September 2013, Accepted 20 November 2013, Scheduled 23 November 2013
* Corresponding author: Cheng Yuan Chin (paladinchin@gmail.com).

gratings with lossy materials have also received considerable attention. Besides planar configuration [3], non-planar applications were also demonstrated using resistive gratings. For instance, the multilayered absorber was bent and applied to the leading edge of a wing-shaped structure [4]. Resistive grating is constructed of periodic resistive sheet with specific pattern, which can be regarded as metallic grating with finite conductivity, and it possesses greater control of the grating's reflection characteristic. In fact, the lossy laminate is made of E-glass fiber/epoxy prepreg containing various kinds of carbon nano materials [5]. The electromagnetic property can be controlled by adding lossy nanofillers to the polymer matrix.

In order to compute scattering and other electromagnetic phenomena in the presence of resistive grating, it is necessary to introduce some simplification to make the problem tractable. Through the use of approximate boundary condition, the complexity and computational expenses of the analysis can be reduced [6]. Impedance and resistive boundary conditions are two remarkable examples. Impedance boundary condition is obtained by considering a plane wave incident on a half plane [7–10], and it is assumed impenetrable. However, the resistive boundary condition is closely related to impedance boundary condition but has partial transparency [11, 12]. The idealized resistive sheet is infinitesimally thin so that the tangential electric fields are the same on both sides. Since it supports electric current at the surface, a discontinuity, referred to as a jump condition, for the tangential magnetic field components across the surface is originally proposed by Levi-Civita [13].

Using resistive boundary condition with a single edge-mode expansion for the strip current, a closed-form solution was derived for the TE mode scattering by a resistive strip array on a dielectric layer [14]. The solution was based on the assumption of small-width strips. Recently, an equivalent anisotropic resistive boundary condition (ARBC) was developed by Whites and Mittra [15]. This ARBC model can be used for infinite or finite periodic objects provided that the structure has rotational symmetry and sufficiently large surface resistance. A more complicated structure in the form of multilayered mushroom-type high impedance surface has been presented and characterized by a simple analytical model [16]. It is a combination of metallic wire medium and resistive patch arrays. This model gives accurate results when the slit between adjacent mushroom structures is much smaller than the periodicity for small and moderate values of surface resistance.

Many different formulations have been considered for analytical solutions to the problem of resistive gratings, and the use of integral

equations and the spectral-Galerkin method are most familiar.

The key processes of the integral equation approach with singular kernel functions are to extract the logarithmic factor of the kernel function, and then using a group of orthogonal eigenfunctions of the singular element as the basis and testing functions in a moment procedure. This is a sophisticated version of traditional moment method, which is regarded as a regularization procedure, since the resultant set of linear algebraic equations is in the form of Fredholm second kind [2, 17].

The spectral-Galerkin method is another approach which has been harnessed successfully to periodic structures with zero thickness for both perfectly conducting and resistive surfaces. In the spectral domain, the convolution form of the integral equation for the scattered field reduces to product form by Fourier transformation. The unknown induced currents on the surface are expanded in a set of basis functions, and the matrix equation with expansion coefficients are then solved by moment method techniques [18, 19].

However, the above methods intend to solve the problem where the unit cell consists of only one kind of resistive strip. If there are more resistive strips having different resistances inside the unit cell, a reformulation process is needed according to the unit cell geometry and the total number of resistive strips. To address the issue, Fourier expansion of inhomogeneous admittance function is used in order to synchronize with the Floquet mode matching analysis.

The paper is organized as follows. Section 2 provides the general formulation of wave scattering by a two-dimensional resistive grating. The concept of Fourier expansion is involved in the resistive boundary condition. Section 3 extends the approach to retrieve the equivalent circuit model of the resistive grating. Two kinds of resistive gratings are investigated. The structure under consideration is confined to one-dimensional periodicity to cope with different features caused by TE and TM polarizations. In Section 4, we demonstrate two numerical examples to validate the accuracy of circuit model. Section 5 summarizes the conclusions [23–25].

2. FORMULATION

In this section, we calculate the reflection and transmission characteristics of a multilayered periodic structure packed in a rectangular array. The structure is formed by a two-dimensional resistive grating sandwiched in two different homogeneous dielectric layers, which is depicted in Figure 1. The numerical analysis is performed based on the resistive boundary condition (RBC). In the

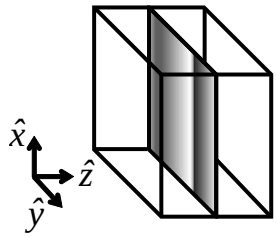

Figure 1. Unit cell of resistive grating inserted in the middle of two distinct dielectric mediums.

following, a time variation of the form $e^{j\omega t}$ is assumed and suppressed, and both transverse electric (TE) and transverse magnetic (TM) polarizations are considered.

As noted by Levi-Civita [13], the RBCs at the resistive surface are

$$\hat{z} \times \left[\underline{E}_t\left(z = 0^+\right) - \underline{E}_t\left(z = 0^-\right)\right] = 0 \tag{1}$$

$$\hat{z} \times \left[\underline{H}_t\left(z = 0^+\right) - \underline{H}_t\left(z = 0^-\right)\right] = \underline{J} \tag{2}$$

and

$$\hat{z} \times \left[\hat{z} \times \underline{E}_t\left(z = 0^{\pm}\right)\right] = -Z_s \cdot \underline{J} \tag{3}$$

where the "+" and "−" signs refer to surfaces just above or below the sheet. Z_s is the surface impedance and J is the induced current on the surface. Equation (1) implies that the tangential electric fields near the sheet in medium 1 and 2 are continuous at $z = 0$, while (2) is analogous to Kirchhoff's current law as shown in Figure 2. Substituting (2) into (3) gives

$$\underline{H}_t\left(z = 0^-\right) - \underline{H}_t\left(z = 0^+\right) = Y_s \cdot \left[\hat{z} \times \underline{E}_t\left(z = 0^{\pm}\right)\right] \tag{4}$$

and Y_s is the inverse of the surface impedance Z_s.

To simulate the electromagnetic properties of such grating, we employ the rigorous coupled wave analysis (RCWA) originally presented by Moharam et al. [20, 21].

In accordance with Floquet's theorem, the tangential electric and magnetic fields within the homogeneous region are written as the Fourier expansion of spatial harmonics given by

$$\begin{aligned} \underline{E}_t &= \sum_{m=-\infty}^{\infty} \sum_{n=-\infty}^{\infty} \underline{e}_{tmn}(z) \cdot \exp(-j(k_{xm}x + k_{yn}y)) \\ \underline{H}_t &= \sum_{m=-\infty}^{\infty} \sum_{n=-\infty}^{\infty} \underline{h}_{tmn}(z) \cdot \exp(-j(k_{xm}x + k_{yn}y)) \end{aligned} \tag{5}$$

and

$$\begin{aligned} k_{xm} &= k \sin\theta \cos\phi + 2\pi m/p_x \\ k_{yn} &= k \sin\theta \sin\phi + 2\pi n/p_y \end{aligned} \tag{6}$$

where $\underline{e}_{tmn}(z)$ and $\underline{h}_{tmn}(z)$ represent the modal amplitudes of spatial harmonics for the electric and magnetic fields, respectively. In (6), k denotes the wave vector, ϕ is the polar angle, and θ is the azimuth angle of the incident plane wave.

In the resistive grating layer, the sheet (located at $z = 0$) is assumed to be infinitely thin and having periodic admittance distribution $Y_s(x, y)$. The period of grating along the x- and y-axes, are denoted by p_x and p_y, respectively. In (4), the Fourier component $Y_{m,n}$ of the admittance distribution $Y_s(x, y)$ is given by

$$Y_{m,n} = \frac{1}{p_x p_y} \int_0^{p_x} \int_0^{p_y} Y_s(x,y) \cdot \exp\left(j\left(\frac{2\pi m}{p_x}x + \frac{2\pi n}{p_y}y\right)\right) dxdy \tag{7}$$

After substituting (5) and (7) into (1) and (4) and collecting the expanded Fourier components leads to

$$\begin{aligned} \underline{e}_{t1} &= \underline{e}_{t2} \\ \underline{h}_{t1} - \underline{h}_{t2} &= \mathbb{Y}_s \underline{e}_{t1} \end{aligned} \tag{8}$$

where

$$\underline{e}_t = \begin{bmatrix} -e_y \\ e_x \end{bmatrix}, \quad \underline{h}_t = \begin{bmatrix} h_x \\ h_y \end{bmatrix} \tag{9}$$

The electric and magnetic field components in (8) is further expressed in terms of eigenvectors in the homogeneous medium which gives

$$\begin{aligned} &\mathbb{Q}_1(\underline{a}_1 + \underline{b}_1) = \mathbb{Q}_2(\underline{a}_2 + \underline{b}_2) \\ &\mathbb{Q}_1\mathbb{Y}_1(\underline{a}_1 - \underline{b}_1) - \mathbb{Q}_2\mathbb{Y}_2(-\underline{a}_2 + \underline{b}_2) = \mathbb{Y}_s\mathbb{Q}_1(\underline{a}_1 + \underline{b}_1) \end{aligned} \tag{10}$$

Parameters $\underline{a}$ and $\underline{b}$ are the incident and reflected wave amplitudes along the z-axis, while the subscript denotes in which medium the fields are. $\mathbb{Q}$ is a square matrix whose i-th column contains the eigenvector $\underline{q}_i$. $\mathbb{Y}_1$ (or $\mathbb{Y}_2$) is a diagonal matrix having the admittance of each eigenvector on its main entry. Specifically, $\mathbb{Y}_s$ is the admittance matrix of the resistive grating, and it will be a full matrix (a tensor) if the resistive grating is inhomogeneous.

Rearranging (10), the scattering matrix is derived as

$$\begin{aligned} \mathbb{S}_{11} &= \left(\mathbb{Q}_1^{-1}\mathbb{Q}_2\mathbb{Y}_2\mathbb{Q}_2^{-1}\mathbb{Q}_1 + \mathbb{Y}_1 + \mathbb{Q}_1^{-1}\mathbb{Y}_s\mathbb{Q}_1\right)^{-1} \\ &\quad \cdot \left(-\mathbb{Q}_1^{-1}\mathbb{Q}_2\mathbb{Y}_2\mathbb{Q}_2^{-1}\mathbb{Q}_1 + \mathbb{Y}_1 - \mathbb{Q}_1^{-1}\mathbb{Y}_s\mathbb{Q}_1\right) \\ \mathbb{S}_{12} &= \left(\mathbb{Q}_1^{-1}\mathbb{Q}_2\mathbb{Y}_2\mathbb{Q}_2^{-1}\mathbb{Q}_1 + \mathbb{Y}_1 + \mathbb{Q}_1^{-1}\mathbb{Y}_s\mathbb{Q}_1\right)^{-1} \cdot \left(2 \cdot \mathbb{Q}_1^{-1}\mathbb{Q}_2\mathbb{Y}_2\right) \\ \mathbb{S}_{21} &= \left(\mathbb{Q}_2^{-1}\mathbb{Q}_1\mathbb{Y}_1\mathbb{Q}_1^{-1}\mathbb{Q}_2 + \mathbb{Y}_2 + \mathbb{Q}_2^{-1}\mathbb{Y}_s\mathbb{Q}_2\right)^{-1} \cdot \left(2 \cdot \mathbb{Q}_2^{-1}\mathbb{Q}_1\mathbb{Y}_1\right) \end{aligned} \tag{11}$$

$$\mathbb{S}_{22} = \left(\mathbb{Q}_2^{-1}\mathbb{Q}_1\mathbb{Y}_1\mathbb{Q}_1^{-1}\mathbb{Q}_2 + \mathbb{Y}_2 + \mathbb{Q}_2^{-1}\mathbb{Y}_s\mathbb{Q}_2\right)^{-1} \cdot \left(-\mathbb{Q}_2^{-1}\mathbb{Q}_1\mathbb{Y}_1\mathbb{Q}_1^{-1}\mathbb{Q}_2 + \mathbb{Y}_2 - \mathbb{Q}_2^{-1}\mathbb{Y}_s\mathbb{Q}_2\right)$$

The scattering matrices in the above equations fully describe the reflection and transmission properties of each eigenmode. And it is intuitive to find the analogy between the sandwiched resistive grating and two transmission lines with a shunt admittance in the middle, which is illustrated in Figure 2. The scattering parameters of the latter case can be derived directly when each matrix on the right-hand side of (11) is replaced by a scalar.

$$\begin{aligned} S_{11} &= (Y_1 + Y_2 + Y_s)^{-1}(Y_1 - Y_2 - Y_s) \\ S_{12} &= (Y_1 + Y_2 + Y_s)^{-1}(2 \cdot Y_2) \\ S_{21} &= (Y_1 + Y_2 + Y_s)^{-1}(2 \cdot Y_1) \\ S_{22} &= (Y_1 + Y_2 + Y_s)^{-1}(-Y_1 + Y_2 - Y_s) \end{aligned} \tag{12}$$

It is a meaningful way to interpret the resistive grating through the equivalent circuit model. When $Y_s = 0$, which means a shunt open circuit is between two transmission lines, no power is consumed by the grating; when $Y_s = \infty$, which means a shunt short circuit is between two transmission lines, the incident wave suffers a total reflection with 180° out of phase at the interface, and this case corresponds to a PEC sheet in reality.

Our custom RCWA code using the Matlab programming environment was employed to compute the complex scattering parameters for such grating. We provide two examples: one is the conventional resistive grating, and the other is the composite resistive grating. The unit cell of conventional resistive grating contains a resistive square patch. Meanwhile, the proposed composite resistive grating is actually the combination of a square patch and a square aperture as shown in Figure 3. The originally void region in conventional resistive grating is now filled with resistive sheet. In fact, the conventional resistive grating can be viewed as a special case

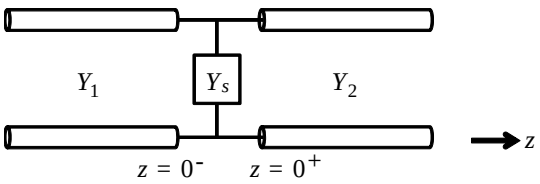

Figure 2. Equivalent transmission line model for structure shown in Figure 1.

of composite one when $R_{sc} = \infty$. In the examples, both gratings are embedded in a medium with relative dielectric constant $\epsilon_r = 2.3$ as shown in Figure 3. Background material also has $\epsilon_r = 2.3$. The admittance distribution is given below.

$$\begin{aligned} Y_s(x,y) &= \tfrac{1}{150}, \quad -\tfrac{w}{2} \leqslant x, y \leqslant \tfrac{w}{2} \\ &= 0, \qquad \text{otherwise (conventional)} \\ &= \tfrac{1}{500}, \quad \text{otherwise (composite)} \end{aligned} \tag{13}$$

Computed magnitudes and phases under both TE and TM incidence for the examples are shown in Figures 4 and 5. The numbers

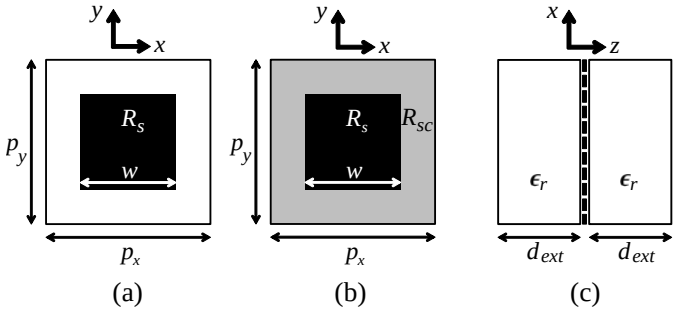

Figure 3. Unit cell of resistive grating in patch geometry. (a) Front view of conventional resistive grating. (b) Front view of composite resistive grating. (c) Side view of the grating.

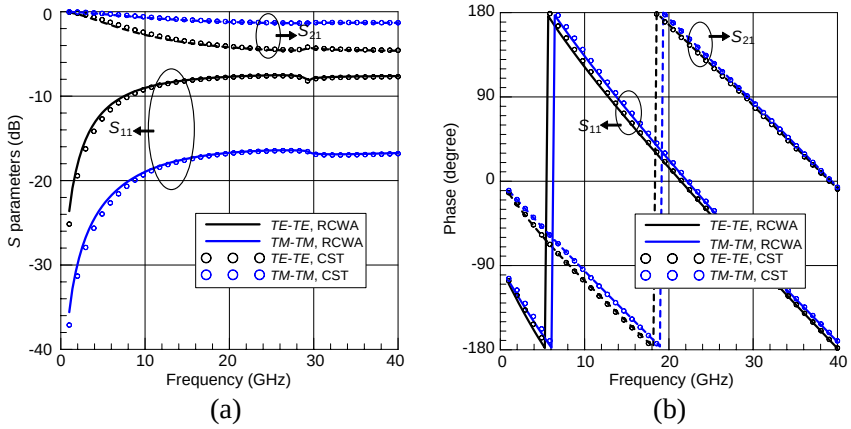

Figure 4. Numerical results of conventional resistive grating shown in Figure 3. $p_x = p_y = 3.6\,\text{mm}$, $w = 2.6\,\text{mm}$, $R_s = 150\,\Omega/\text{square}$, $\epsilon_r = 2.3$, $d_{ext} = 5\,\text{mm}$, $\phi = 0°$, $\theta = 60°$. (a) Magnitude. (b) Phase.

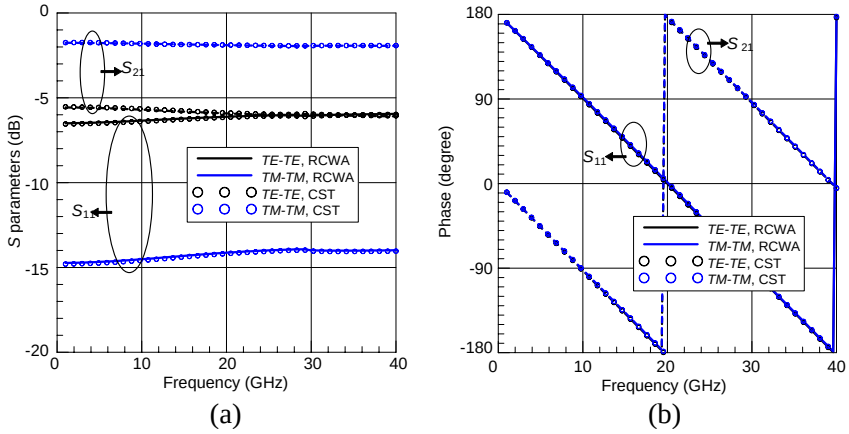

Figure 5. Numerical results of composite resistive grating shown in Figure 3. $p_x = p_y = 3.6\,\text{mm}$, $w = 2.6\,\text{mm}$, $R_s = 150\,\Omega/\text{square}$, $R_{sc} = 500\,\Omega/\text{square}$, $\epsilon_r = 2.3$, $d_{ext} = 5\,\text{mm}$, $\phi = 0°$, $\theta = 60°$. (a) Magnitude. (b) Phase.

of Fourier orders (m, n) used in the examples are from -15 to 15. The results from RCWA are compared with the commercial code CST Microwave Studio and show little disagreement. Note that this example suffers the Gibb's phenomenon using only 31 modes, but it is unobvious in virtue of the small contrast $(1/150 - 0 = 1/150)$ in the periodic admittance function. The mode number used here is a compromise between the calculation accuracy and the matrix dimension in (11). The matrix dimension also affects the time consumption and memory storage requirements during calculation.

3. EQUIVALENT CIRCUIT MODEL AND COMPUTED RESULTS

The purpose of this section is to derive the equivalent circuit model based on the formulation reported previously. Although the numerical analysis of a two-dimensional periodic resistive grating has been established, the equivalent circuit model extraction is only aimed at one-dimensional grating in this paper. For 1D periodic structure, the scattering characteristics depend on the polarization of incidence, so the equivalent circuit model extraction for TE and TM modes are considered independently. We define that p is the period along the x-axis, and the fields are independent of y $(\partial/\partial y = 0)$. Thus, the waves can be individually decomposed into TE_z $(E_z = 0)$ and TM_z

($H_z = 0$).

To increase the accuracy of circuit model extraction in the periodic structure, the grating period p must be sufficiently small compared to the incident wavelength ($\lambda_0/\sqrt{\epsilon_r}$) such that only the fundamental diffractive order ($m = 0$) will propagate while other higher-order modes will be evanescent. This condition is written mathematically as

$$p < \frac{\lambda_0/\sqrt{\epsilon_r}}{1 + \sin\theta} \tag{14}$$

where θ is the azimuth angle of the incident plane wave on XZ plane.

In the following, the conventional and composite resistive gratings will be investigated numerically. The grating is embedded in the middle of air ($\epsilon_r = 1$), as shown in Figure 6, and is illuminated by a normally incident plane wave. The period p of unitcell is 3.6 mm and the calculation domain of frequency is from 1 to 40 GHz. Diffractive order (m) for 1D RCWA calculation is from -240 to 240 through this paper.

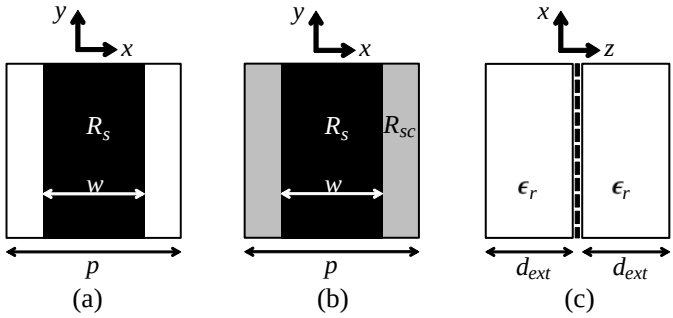

Figure 6. Unit cell of resistive grating in strip geometry. The structure is infinite in y-direction. (a) Front view of conventional resistive grating. (b) Front view of composite resistive grating. (c) Side view of the grating.

Using the RCWA code, the complete scattering matrix of the structure shown in Figure 1 can be obtained. Then, a single-mode extraction is performed by keeping the results of matrix element from fundamental modes (0th-0th order) while neglecting the others. Subsequently, the original matrix is reshaped into a 2-by-2 matrix, and the equivalent admittance of the grating can be retrieved for the given circuit model. The scattering matrix of the circuit model shown in Figure 2, where the RLC values involved in Y_s are unknowns, is employed for curve fitting with the previous 2-by-2 scattering matrix.

We have investigated the relation between mode number and the admittance function through convergence test. When the filling ratio w/p (shown in Figures 3 and 6) is close to 0 or 1, indicating narrow strip or narrow gap, or the contrast of the two-tone admittance function $(1/R_s - 1/R_{sc})$ is too large, these situations will lead to slow convergence and more modes should be considered for computation. In the two-dimensional case of Section 2, we intend to demonstrate the validity of our RCWA code via comparison with commercial software. Therefore, we choose the admittance function (shown in (13)) with medium filling ratio and low contrast, so 31 Fourier modes are sufficient to give a harsh but accurate results. However, in the one-dimensional case of the following subsections, the minimum value of filling ratio taken into account in Figure 8 is 0.0278, which requires at least 481 Fourier modes to satisfy our convergence criterion. The mode number can be reduced if we increase the considered minimum filling ratio.

3.1. Conventional Resistive Grating

Referring to the conventional resistive grating illustrated in Figure 7, it transforms into PEC strip grating when R_s is set to zero, and its equivalent circuit model was reported by Marcuvitz [22] in the form of either a shunt capacitance or shunt inductance. To characterize the resistive grating instead of PEC grating, the lumped element R has been added into the model which accounts for the lossy property.

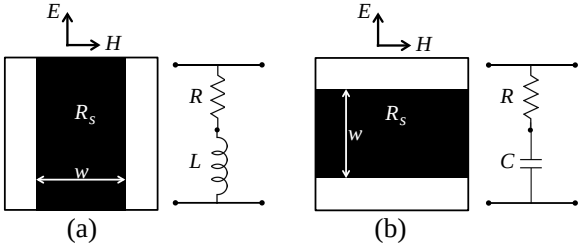

Figure 7. The equivalent circuit models of conventional resistive grating for (a) TE and (b) TM polarizations.

The extracted values of circuit model are affected by two variables, the surface resistance R_s and filling ratio w/p. To visualize the relationship between the physical dimensions and extracted RLC values, either the surface resistance or the filling ratio is swept while keeping the other one constant. In Figure 8, low filling ratio results in large inductance for TE mode but small capacitance for TM mode. Note that when the filling ratio approaches zero, the

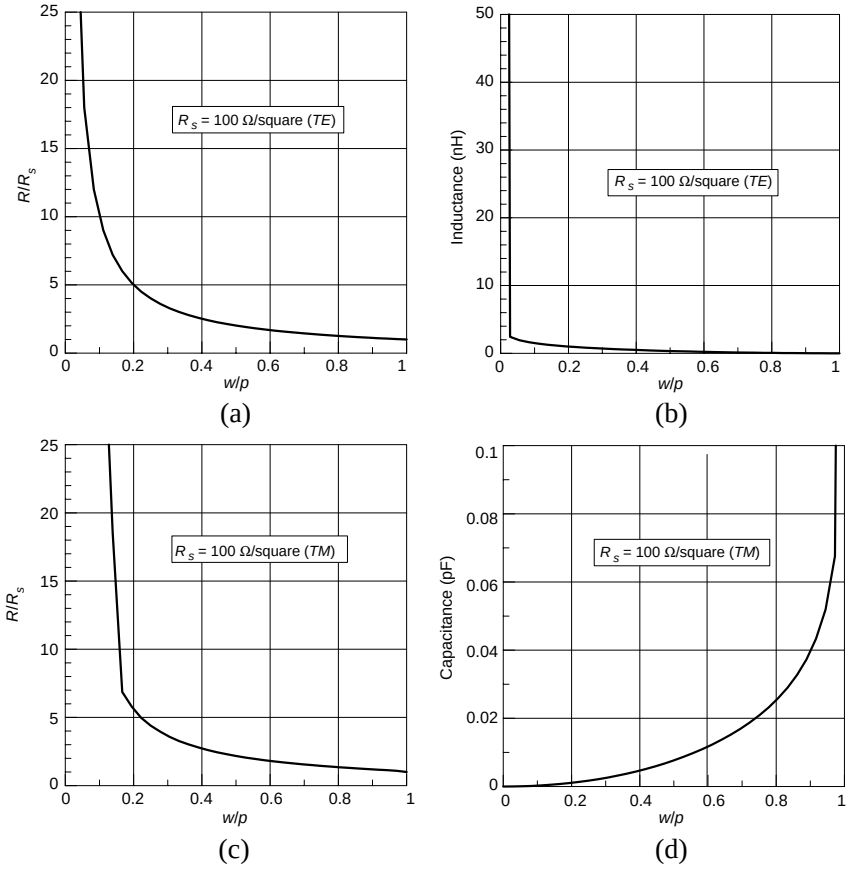

Figure 8. The extracted RLC values against filling ratio while $R_s = 100\,\Omega$/square. (a) TE mode: R/R_s. (b) TE mode: L. (c) TM mode: R/R_s. (d) TM mode: C.

impedance approaches infinity because the resistive sheet is about to disappear physically, and the circuit model becomes a shunt open circuit. However, when the filling ratio approaches one, the reactance will be zero, and thus leads to a homogeneous condition $R = R_s$. This condition applies to both TE and TM modes.

Figure 9 reveals that, by sweeping the surface resistance R_s, the reactance is nearly constant for TM mode and drops slightly for TE mode if R_s is small. This is a useful property in realizing actual RL or RC circuits. Since changing R_s doesn't affect the inductance or capacitance substantially, the required sheet reactance can be

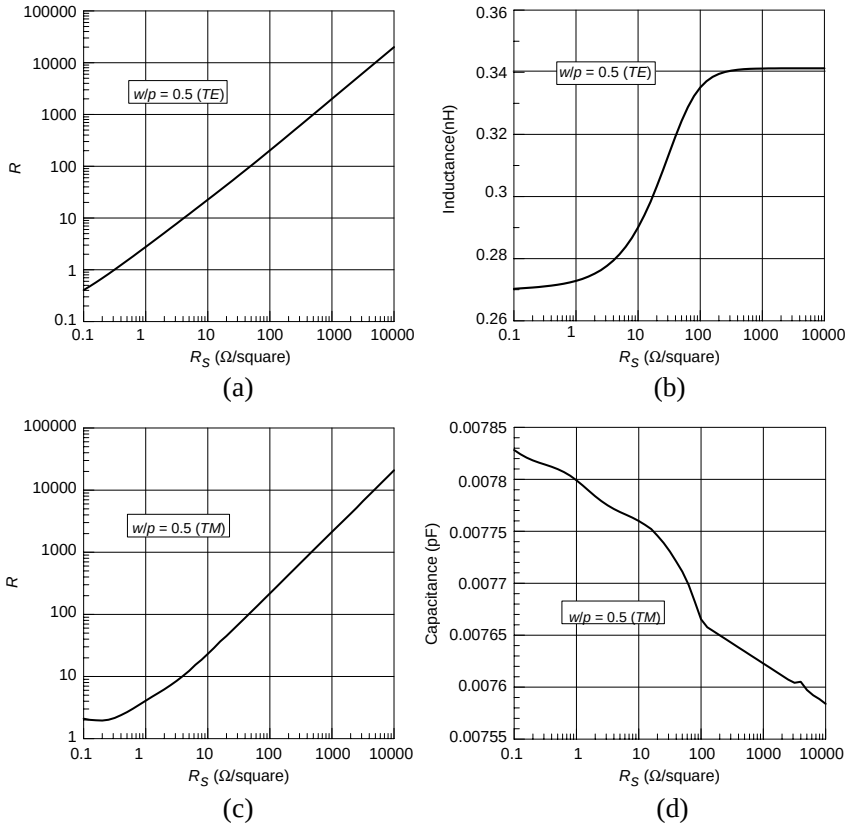

Figure 9. The extracted RLC values against surface resistance while $w/p = 0.5$. (a) TE mode: R. (b) TE mode: L. (c) TM mode: R. (d) TM mode: C.

synthesized by considering only the filling ratio of periodic strips. On the contrary, the extracted resistance is a monotonically increasing function of R_s, and it ranges between zero and positive infinity, which correspond to PEC strip grating and open circuit, separately.

3.2. Composite Resistive Grating

To clarify the composite resistive grating, it can be viewed as the combination of two complementary conventional resistive gratings with different surface resistances. Specifically, there is no blank space inside the composite resistive grating. It is regarded as an intermediate between the homogeneous resistive sheet and conventional resistive

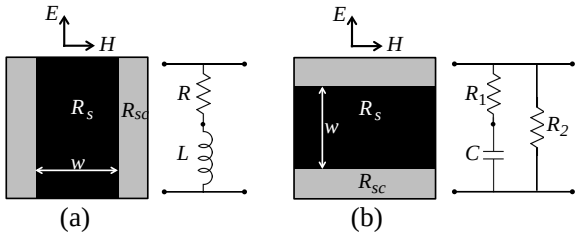

Figure 10. The equivalent circuit models of composite resistive grating for (a) TE and (b) TM polarizations.

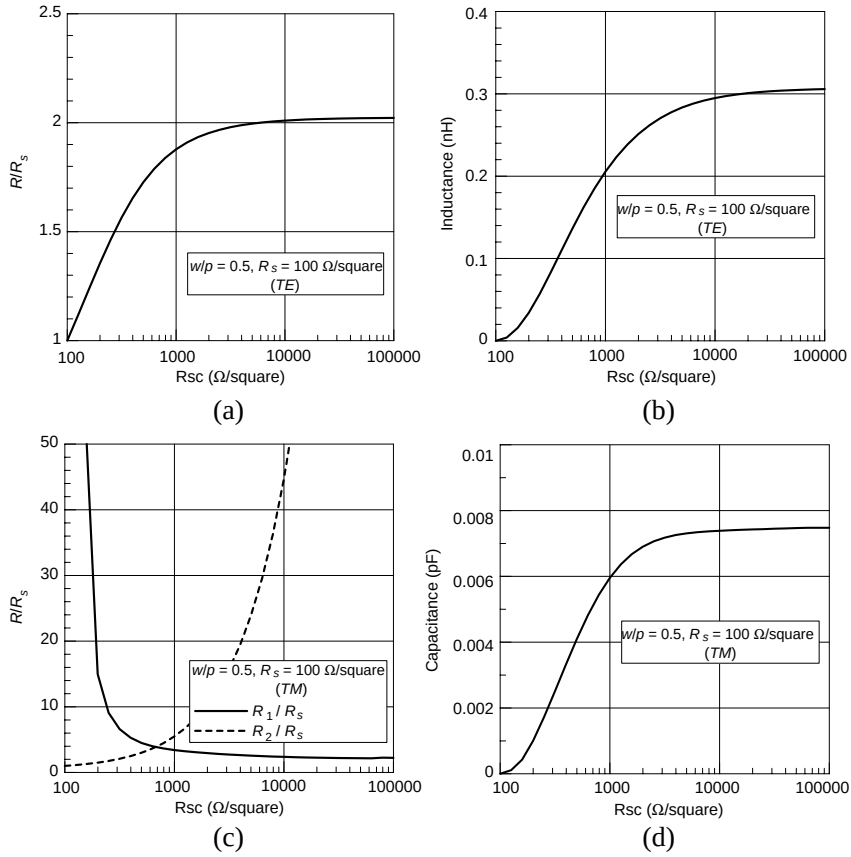

Figure 11. The extracted RLC values against complementary surface resistance while $w/p = 0.5$ and $R_s = 100\,\Omega$/square. (a) TE mode: R/R_s. (b) TE mode: L. (c) TM mode: R_1/R_s and R_2/R_s. (d) TM mode: C.

grating, which can be easily verified by substituting R_s or infinity into R_{sc} in Figure 6. Since a new variable R_{sc} appears, we can infer that one more lumped element is required in the equivalent circuit model. After a sequence of trial and error, we discover that adding a shunt resistance in the original circuit model is sufficient to describe the composite grating, as depicted in Figure 10. However, the second resistance appears ineffective for TE mode, so its circuit model remains the same. The new form of circuit model for TM mode is relatively complex, so the curve fitting technique is applied to retrieve the equivalent lumped element values.

For the succinctness of this paper, only R_{sc} is swept in this subsection since varying R_s and w/p will give similar results as discussed previously. The lower bound of R_{sc} is chosen to be R_s in order not to overlap other cases. For example, if w/p is 0.5, R_s is 100, and R_{sc} is 50, it is equal to another case where R_s is 50 and R_{sc} is 100.

Figure 11 exhibits that the extracted impedance starts from a pure resistance and then approaches a constant complex value progressively when R_{sc} varies from R_s to $1000R_s$ for both TE and TM modes. Particularly, the behavior of circuit model for TM mode is explicitly discussed in next paragraph.

As shown in Figure 12, in the homogeneous condition ($R_{sc} = R_s$), the capacitance becomes zero, and the effect of R_2 predominates the whole circuit. On the other hand, when R_{sc} is much greater than R_s, both R_1 and C converge to constants while R_2 becomes an extremely large number which can be neglected in the circuit model. In general, the RCR circuit model will degenerate into either R or RC depending on the value of complementary surface resistance.

To obtain the explicit impedance formula for RLC circuit will be useful, but it is beyond the scope of this paper. However, the interested readers may refer to [14] for more detail. The closed-from expression for complex resistivity of periodic resistive strip array has been derived for

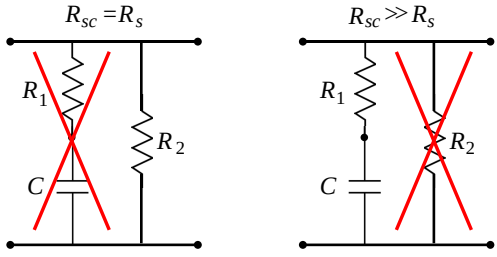

Figure 12. The behavior of RCR circuit model when R_{sc} is equal to or much greater than R_s.

TE scattering. Although this approach can provide physical insights for the circuit analysis, it is less accurate than the proposed RCWA method, since the solution is based on the assumption of small-width strips and single edge-mode for the strip current.

4. NUMERICAL EXAMPLES

For years, the circuit analog absorbers using resonating FSS elements investigated by Munk [23–25] were believed to outperform the conventional Jaumann absorbers regarding the bandwidth and thickness. The bandwidth ratio of 10 : 1 as a figure of merit has been claimed by Munk [24] without any evidence. Due to the resonating characteristic of FSS element, the harmonics of fundamental resonance, which occur at frequencies 2 or 3 times higher than the intrinsic resonating frequency, must be taken into account in the wideband absorber design. Therefore, designing a circuit analog absorber with bandwidth over 10 : 1 incorporating FSS would be a complicated task and has not yet been reported in public literature.

The absorber design for oblique incidence angle using Smith chart is explored [24, 25], but it is restricted to only one resistive layer, and this method is expected to be modified for multilayered case. Since numerous parameters are involved in a multilayered absorber design, and oblique incidence for both polarizations leads to a multi-objective problem, the Smith chart matching technique suggested by Munk becomes infeasible to handle. Consequently, the computer optimization with educated guesses serves as the best strategy to accomplish the design process.

The main purpose of this research is aimed at the characterization of composite resistive grating rather than designing an ultra-wideband absorber for oblique angle of incidence. Although our approach employing RC or RCR elements can provide a reasonable solution achieving all the requirements stated above, the detail is omitted in this paper.

In this section, we present two examples of multilayered Jaumann absorbers. The structure is based on the work of Kazemzadeh and Karlsson [3], and the proposed composite resistive grating is employed and integrated into the absorber. The schematic of the Jaumann absorber is depicted in Figure 13. Type A and Type B represent conventional resistive grating and composite resistive grating, respectively. All the resistive sheets are inserted in the middle of identical dielectric covers in purple. Note that there are three kinds of resistive gratings for each type. The first resistive layer is a homogeneous sheet, the second layer is a resistive grating with period

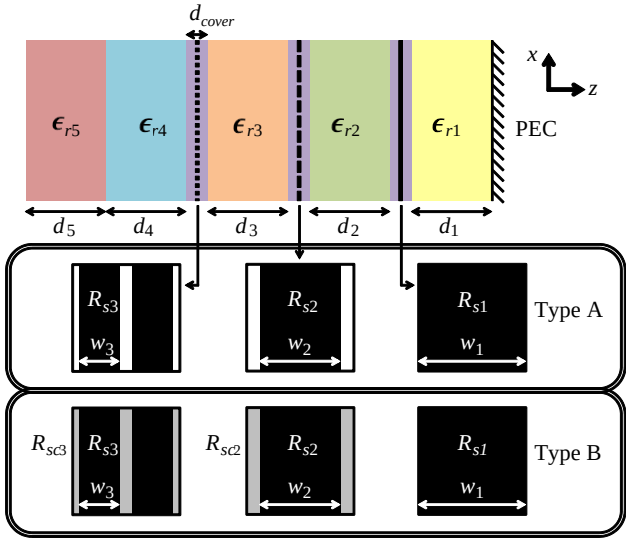

Figure 13. The schematic of the multilayered Jaumann absorber incorporating conventional (type A) or composite (type B) resistive gratings. The parameters are listed in Tables 1 and 3.

Table 1. Parameters of each dielectric layer and dielectric cover.

	Homogeneous Dielectric Layer					Dielectric
	Layer 1	Layer 2	Layer 3	Layer 4	Layer 5	Cover
d (mm)	3.4	2.6	2.4	3.3	4	0.4
ϵ_r	1.8	1.7	1.33	1.8	1.33	2.3

p, and the third one is also a resistive grating but with period $p/2$. In this design, the parameters of the dielectric layers are tabulated in Table 1.

The lumped values of the whole structure are obtained through optimization process and listed in Table 2. Note that the goal of optimization is to achieve a -20 dB absorptivity from 5 to 30 GHz for TM incident wave. To convert the lumped circuit model into the dimension and surface resistance of a practical resistive grating, we need to proceed root finding procedure. The charts in Figures 8–11 can help us determine appropriate initial guesses. The synthesized values are shown in Table 3.

For TM polarization, the conventional resistive grating is regarded as a low-pass RC element, and is an appropriate candidate for ultra-

Table 2. Optimized values of the equivalent circuit model in each resistive layer.

		TM		
		Layer 1	Layer 2	Layer 3
Type A	R (Ω)	148.77	359.32	612.73
	C (pF)	-	0.13481	0.02763
Type B	R_1 (Ω)	154.89	398.72	798.27
	R_2 (Ω)	-	3036.62	1142.71
	C (pF)	-	0.06377	0.01278

Table 3. Synthesized parameters of each resistive layer.

		Resistive Layer		
		Layer 1	Layer 2	Layer 3
Type A	R_s (Ω/square)	148.77	336.37	460.87
	w (mm)	3.6	3.5	1.45
Type B	R_s (Ω/square)	154.89	297.75	354.16
	R_{sc} (Ω/square)	-	32499.37	4021.52
	w (mm)	3.6	3.2	1.4

wideband absorber design. However, there are some restrictions to realize a large capacitance in reality. One way is to embed the resistive grating into a medium with high dielectric constant, which increases the equivalent capacitance but introduces higher-order propagating modes that destroys the consistency between circuit model and grating. Another solution is to reduce the gap width between resistive strips, and this factor is directly influenced by the accuracy of manufacturing process. In the current example, the gap width for Type A at the second resistive layer is only 0.1 mm in order to synthesize a capacitance of 0.135 pF, shown in Tables 2 and 3. Specifically, a novel RCR element is presented in this paper, which can be practically realized by the composite resistive grating, and it provides more degrees of freedom for absorber design. Namely, the same absorbing performance can be accomplished while large capacitance is unnecessary. In the current design, the minimal gap width of composite resistive grating is extended to 0.4 mm. Therefore, the proposed grating has higher tolerance against deviations from realistic fabrication comparing to conventional one.

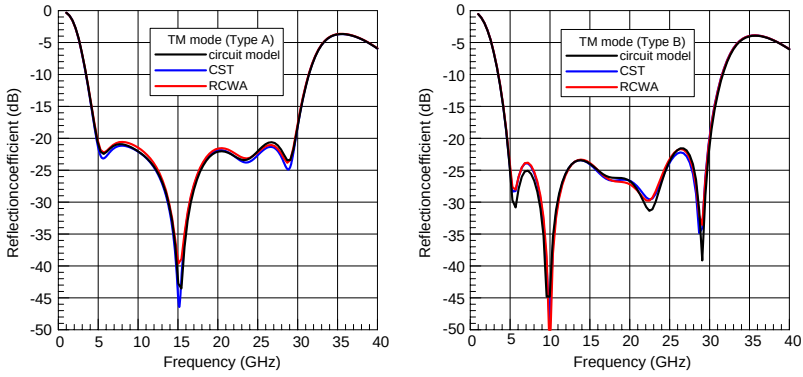

Figure 14. The reflection coefficients of Jaumann absorbers shown in Figure 13 under normal incidence ($\theta = 0°$) with TM polarization. (a) Type A. (b) Type B.

Figure 14 shows very close agreement between the frequency responses calculated from the equivalent circuit model, full-wave simulation (CST Microwave Studio), and RCWA. This is unlikely to happen unless the resistive gratings have been modeled with very high accuracy.

5. CONCLUSION

In this paper we present a novel composite resistive grating. It is similar to the conventional resistive grating, but with two different surface resistances. Based on the RBC, the general formulation to calculate the scattering parameters of two-dimensional resistive gratings is obtained. Different from spectral domain analysis using periodic Green's function, the proposed method based on Fourier series expansion can handle resistive grating with arbitrary admittance distribution. Both conventional and composite resistive gratings with 1D periodicity are analyzed and characterized by equivalent circuit models. Design examples of multilayered Jaumann absorbers are demonstrated to validate the consistency between resistive grating and corresponding circuit model. Moreover, the composite resistive grating can provide more degrees of freedom for absorber design.

ACKNOWLEDGMENT

The corresponding author of this paper would like to acknowledge CST^{TM} and Eric Chang (CST Taiwan) for their consistent support.

APPENDIX A. DERIVATION OF (12)

We consider the transmission line model shown in Figure 2. Using Kirchhoff's voltage and current law gives

$$\begin{aligned} V_1 &= V_2 \\ I_1 - I_2 &= Y_s V_1 \end{aligned} \tag{A1}$$

The quantity of voltage and current can be separated into transmitted and reflected parts.

$$a_1 + b_1 = a_2 + b_2 \tag{A2}$$

$$Y_1(a_1 - b_1) - Y_2(-a_2 + b_2) = Y_s(a_1 + b_1) \tag{A3}$$

First we transpose (A2)

$$b_2 = a_1 + b_1 - a_2 \tag{A4}$$

and then substitute (A4) into (A3), which results in

$$(Y_1 + Y_2 + Y_s)b_1 = (Y_1 - Y_2 - Y_s)a_1 + 2Y_2 a_2 \tag{A5}$$

Similarly, transposing (A2) again

$$b_1 = a_2 + b_2 - a_1 \tag{A6}$$

After substitution, the term b_1 is also eliminated.

$$(Y_1 + Y_2 + Y_s)b_2 = 2Y_1 a_1 + (-Y_1 + Y_2 - Y_s)a_2 \tag{A7}$$

Rearranging (A5) and (A7) leads to the complete description of scattering matrix (12) for Figure 2.

REFERENCES

1. Uchida, K., T. Noda, and T. Matsunaga, "Spectral domain analysis of electromagnetic wave scattering by an infinite plane metallic grating," *IEEE Trans. Antennas Propag.*, Vol. 35, No. 1, 46–52, 1987.
2. Matsushima, A. and T. Itakura, "Singular integral equation approach to plane wave diffraction by an infinite strip grating at oblique incidence," *Journal of Electromagnetic Waves and Applications*, Vol. 4, No. 6, 505–519, 1990.
3. Kazemzadeh, A. and A. Karlsson, "Multilayered wideband absorbers for oblique angle of incidence," *IEEE Trans. Antennas Propag.*, Vol. 58, No. 11, 3637–3646, 2010.
4. Choi, W., J. Shin, T. Song, J. Kim, W. Lee, Y. Joo, and C.-G. Kim, "Design of thin circuit-analogue multilayer absorber and application to leading edge of wing structure," *Electron. Lett.*, Vol. 49, No. 3, 216–217, 2013.

5. Kim, J.-B. and J.-H. Byun, "Salisbury screen absorbers of dielectric lossy sheets of carbon nanocomposite laminates," *IEEE Trans. Electromagn. Compat.*, Vol. 54, No. 1, 37–42, 2012.
6. Senior, T. B. A., "Approximate boundary conditions," *IEEE Trans. Antennas Propag.*, Vol. 29, No. 5, 826–829, 1981.
7. Leontovich, M. A., *Investigations on Radiowave Propagation, Part II,* Academy of Sciences, Moscow, 1948.
8. Senior, T. B. A., "Impedance boundary conditions for imperfectly conducting surfaces," *Appl. Sci. Res., Sec. B*, Vol. 8, No. 1, 418–436, 1960.
9. Hwang, R.-B., "Scattering characteristics of two-dimensionally periodic impedance surface," *IEEE Trans. Antennas Propag.*, Vol. 48, No. 10, 1521–1527, 2000.
10. Hwang, R.-B., "Periodic impedance surface," *Periodic Structures: Mode-matching Approach and Applications in Electromagnetic Engineering*, 1st Edition, Chapter 6, 277–280, IEEE Press, John Wiley & Sons, Inc., 2012.
11. Senior, T. B. A., "Backscattering from resistive strips," *IEEE Trans. Antennas Propag.*, Vol. 27, No. 6, 808–813, 1979.
12. Senior, T. B. A., "Combined resistive and conductive sheets," *IEEE Trans. Antennas Propag.*, Vol. 33, No. 5, 577–579, 1985.
13. Bateman, H., *Electrical and Optical Wave Motion*, Cambridge University Press, 1955.
14. Volakis, J., Y.-C. Lin, and H. Anastassiu, "TE characterization of resistive strip gratings on a dielectric slab using a single edge-mode expansion," *IEEE Trans. Antennas Propag.*, Vol. 42, No. 2, 205–212, 1994.
15. Whites, K. and R. Mittra, "An equivalent boundary-condition model for lossy planar periodic structures at low frequencies," *IEEE Trans. Antennas Propag.*, Vol. 44, No. 12, 1617–1629, 1996.
16. Padooru, Y., A. Yakovlev, C. S. R.Kaipa, G. Hanson, F. Medina, F. Mesa, and A. Glisson, "New absorbing boundary conditions and analytical model for multilayered mushroom-type metamaterials: Applications to wideband absorbers," *IEEE Trans. Antennas Propag.*, Vol. 60, No. 12, 5727–5742, 2012.
17. Zinenko, T., A. Nosich, and Y. Okuno, "Plane wave scattering and absorption by resistive-strip and dielectric-strip periodic gratings," *IEEE Trans. Antennas Propag.*, Vol. 46, No. 10, 1498–1505, 1998.
18. Hall, R. and R. Mittra, "Scattering from a periodic array of resistive strips," *IEEE Trans. Antennas Propag.*, Vol. 33, No. 9,

1009–1011, 1985.

19. Hall, R., R. Mittra, and K. Mitzner, "Scattering from finite thickness resistive strip gratings," *IEEE Trans. Antennas Propag.*, Vol. 36, No. 4, 504–510, 1988.
20. Moharam, M. G. and T. K. Gaylord, "Rigorous coupled-wave analysis of planar-grating diffraction," *J. Opt. Soc. Am.*, Vol. 71, No. 7, 811–818, 1981.
21. Moharam, M. G., E. B. Grann, D. A. Pommet, and T. K. Gaylord, "Formulation for stable and efficient implementation of the rigorous coupled-wave analysis of binary gratings," *J. Opt. Soc. Am. A*, Vol. 12, No. 5, 1068–1076, 1995.
22. Marcuvitz, N., *Waveguide Handbook*, McGraw-Hill, New York, 1951.
23. Munk, B. A., *Frequency Selective Surfaces: Theory and Design*, Wiley, New York, 2000.
24. Munk, B. A., P. Munk, and J. Pryor, "On designing Jaumann and circuit analog absorbers (CA absorbers) for oblique angle of incidence," *IEEE Trans. Antennas Propag.*, Vol. 55, No. 1, 186–193, 2007.
25. Munk, B. A., *Metamaterials: Critique and Alternatives*, Wiley, New York, 2009.